Lab on a Chip

View Online
Dynamic Article Links

Cite this: *Lab Chip*, 2011, **11**, 1786

www.rsc.org/loc

PAPER

A microfluidic-based hydrodynamic trap: design and implementation†

Melikhan Tanyeri,[a] Mikhil Ranka,[a] Natawan Sittipolkul[a] and Charles M. Schroeder*[ab]

Received 20th December 2010, Accepted 15th March 2011
DOI: 10.1039/c0lc00709a

We report an integrated microfluidic device for fine-scale manipulation and confinement of micro- and nanoscale particles in free-solution. Using this device, single particles are trapped in a stagnation point flow at the junction of two intersecting microchannels. The hydrodynamic trap is based on active flow control at a fluid stagnation point using an integrated on-chip valve in a monolithic PDMS-based microfluidic device. In this work, we characterize device design parameters enabling precise control of stagnation point position for efficient trap performance. The microfluidic-based hydrodynamic trap facilitates particle trapping using the sole action of fluid flow and provides a viable alternative to existing confinement and manipulation techniques based on electric, optical, magnetic or acoustic force fields. Overall, the hydrodynamic trap enables non-contact confinement of fluorescent and non-fluorescent particles for extended times and provides a new platform for fundamental studies in biology, biotechnology and materials science.

Introduction

Trapping and manipulation of single particles and molecules has enabled remarkable progress in many fields of science and engineering. Over the past several years, a diverse set of tools has been developed to manipulate particles in solution by direct control of their position and velocity. Particle manipulation techniques commonly rely on application of force fields, including optical,[1–4] electric,[5–8] magnetic,[9,10] acoustic,[11,12] and hydrodynamic forces[13–24] in order to confine micro- and nanoscale particles. Each manipulation method has advantages and limitations as a manipulation tool for living cells and biological systems, where perturbations need to be minimized for viability of biological systems.

Particle trapping using hydrodynamic forces was first demonstrated by G. I. Taylor in 1934.[13] Taylor developed a "four-roll mill" apparatus to study dynamics and breakup of macroscopic, millimetre-sized oil droplets in linear viscous flows. Several years later, Bentley and Leal[14] developed a computer-controlled version of the four-roll mill to study particle and droplet dynamics in flow and reported confinement of macroscopic droplets (typically 1 mm diameter) to within 0.5–1.0 mm of the trap center for shear rates up to 5 s^{-1}. Recently, a microfluidic version of the four-roll mill was reported by Hudson *et al.* and Lee *et al.*,[17–19] and these studies mainly focused on the generation of linear mixed flows with a well-defined flow character ranging between simple shear flow and extensional flow in a microfluidic device. Using these devices, large carbon nanotube flocs (typically ~100 μm in size) were studied in viscous (500 cP) polymer solutions.[18]

Recent efforts have focused on combining particle confinement and manipulation methods into integrated devices in order to capitalize on microfluidic technology.[25,26] Several methods employ hydrodynamic forces for capturing and/or manipulating cells or particles and can be classified into two categories: contact-based[27–33] and non-contact[13–24] methods. Contact-based methods use fluid flow to immobilize and physically confine particles against microfabricated obstacles or channel walls,[27–33] whereas non-contact methods rely on stagnation point flows,[13–19] microvortices and microeddies.[21,22] Contact-based methods are efficient in trapping large numbers of particles in an array format for high-throughput studies, however the ability for fine-scale manipulation of individual particles is limited. Non-contact particle confinement methods based on stagnation point flows can provide high resolution manipulation of single particles, though previous work has largely focused on trapping macroscopic particles in aqueous solutions.[13,14]

Microfluidic-based stagnation point flows have also been used to study the dynamics of single DNA molecules. DNA dynamics were characterized in a passive stagnation point flow without the active feedback control[15] and in a stagnation point flow with the human-facilitated manual feedback control.[16,23] However, these microfluidic-based approaches are not practical for precise or long-term confinement of particles in solution due to finite

[a]*Department of Chemical and Biomolecular Engineering, University of Illinois Urbana-Champaign, 600 S. Mathews Ave., Urbana, IL, USA. E-mail: cms@illinois.edu; Fax: +1 (217) 333-5052; Tel: +1 (217) 333-3906*

[b]*Center for Biophysics and Computational Biology, University of Illinois Urbana-Champaign, Urbana, IL, USA*

† Electronic supplementary information (ESI) available: We provide the theoretical calculations describing the effect of constriction width, height and length on the relative flow rates through outlet channels. In addition, we provide the details for the experimental determination of the stagnation point position and the relative flow rates through outlet channels. See DOI: 10.1039/c0lc00709a

residence times in passive flows, where particles ultimately escape into the flowing solution.

Here, we report a microfluidic-based hydrodynamic trap for free-solution particle confinement and manipulation. Hydrodynamic trapping is based on the sole action of fluid flow in a microfluidic device. The hydrodynamic trap is automated and facilitates high resolution, non-contact confinement of micro- and nanoscale particles in a stagnation point flow. The underlying principle of the hydrodynamic trap is the active feedback control of the fluid flow in order to maintain particle center-of-mass position at the trap center. The hydrodynamic trap consists of a simple integrated, two-layer microfluidic device and achieves particle trapping without the need for complex device synthesis or coupling of external fields (optical, electric, or magnetic) into the device.

In this work, we characterize key microfluidic device design parameters for efficient trap performance. We systematically study hydrodynamic trap response as a function of device properties, including membrane valve thickness and stiffness, and channel dimensions. We develop theoretical models for the response of the fluid stagnation point as a function of valve cross-sectional area and applied pressure to the membrane valve, and in all cases, we validate theoretical expressions with experimental measurements. Overall, proper understanding of trap response is essential for engineering and implementing microfluidic-based hydrodynamic traps.

Hydrodynamic trapping: mechanism and control

The hydrodynamic trap is based on the active control of a stagnation point flow generated at a cross-slot junction in a PDMS-based microfluidic device (Fig. 1). Two opposing laminar streams converge at the cross-slot junction and exit through perpendicular outlet channels (Fig. 1c), thereby creating a planar extensional flow, which is a two-dimensional flow containing a fluid stagnation point (zero-velocity point). Planar extensional flows consist of purely extensional and compressional components with no rotational flow character. In the vicinity of the microchannel junction, the fluid velocity is given by:

$$\boldsymbol{u} = \dot{\varepsilon}(-x,y) \tag{1}$$

where $\boldsymbol{u}$ is the velocity vector, $\dot{\varepsilon}$ is the strain rate and (x,y) are the coordinates along the inlet (compressional) and outlet (extensional) directions, respectively, with the origin located at the stagnation point. In a planar extensional flow, the magnitude of the fluid velocity is proportional to the distance from the stagnation point along each component direction.

The key concept behind hydrodynamic trapping is active control of the stagnation point position, thereby enabling dynamic and precise control of the hydrodynamic force exerted on a particle by the fluid. In this way, the flow field is actively controlled to confine and maintain a particle at the fluid stagnation point, which allows for trapping and manipulation of particles in free-solution.

Using the hydrodynamic trap, single micro- and nanoscale particles are trapped at a predetermined target position (trap center) in the microchannel junction. Consider a freely suspended particle entering the cross-channel geometry in the vicinity of the stagnation point. Initially, the particle follows a pathline determined by the hyperbolic fluid streamlines (Fig. 1c). Upon activating the trap, the particle is confined at the trap center by successive iteration of the following experimental

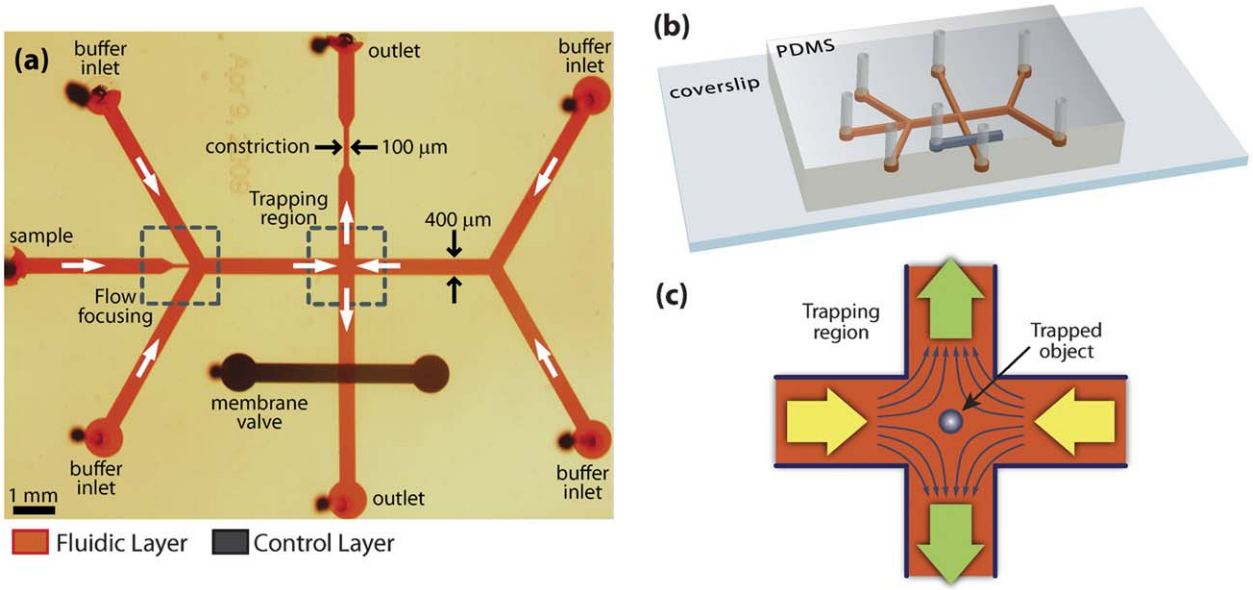

Fig. 1 Microfluidic trapping device. (a) Optical micrograph of a microfluidic trapping device. Sample is introduced *via* flow focusing. Particles in the sample are confined at a predetermined target location at the junction of two perpendicular microchannels (trapping region). A membrane valve positioned above one of the outlet channels is used as a metering valve to control the relative flow rates through the outlet channels. The on-chip valve enables fine-scale control of the stagnation point position, which enables particle trapping. (b) 3-D illustration of the microfluidic trapping device consisting of two device layers in PDMS; the control layer (dark blue) is positioned above the fluidic layer (orange) and acts as a metering valve to adjust the flow rate through the outlet channel underneath (constriction on the outlet not shown). (c) Schematic of the trapping region. Two opposing laminar streams meet at the intersection of two perpendicular microchannels, thereby creating a well-defined flow field containing a stagnation point where an object is trapped.

steps: (i) the centroid position of the particle is determined by image acquisition and image analysis, (ii) a feedback controller determines an updated stagnation point position in order to exert a hydrodynamic force on the particle directing it toward the trap center, and (iii) the stagnation point is re-positioned and the particle moves toward the trap center. In this manner, the stagnation point position is continuously adjusted in order to "steer" a particle towards the trap center. After the particle reaches the trap center, the particle is confined at the stagnation point. In an ideal trap, a particle positioned precisely at the stagnation point achieves zero velocity at the trap center. However, micro- and nanoscale particles are subject to thermal fluctuations and may become displaced by Brownian motion or small perturbations in the flow field, thereby requiring active feedback control.

The stagnation point represents a point of minimum (maximum) flow potential along the inlet (outlet) streams. Therefore, a particle experiences an attractive potential toward the stagnation point along the inlet channel direction and a repulsive potential along the outlet direction with respect to the stagnation point. To achieve particle trapping, it is sufficient to manipulate the stagnation point position along the outflow axis. In this way, the stagnation point is actively re-positioned such that the particle is situated between the trap center and the stagnation point, thereby yielding a hydrodynamic restoring force exerted on the particle in the direction of the trap center. Using this method, particles are confined in two-dimensions by implementing active feedback control in a single direction, corresponding to the outlet (extensional) flow direction in the microfluidic device.

The stagnation point position is actively controlled along the outflow direction *via* an integrated, on-chip valve by adjusting the relative flow rates in the two outlet channels. In this work, we utilize a single membrane valve located on one of the outlet channels (Fig. 1) to effectively manipulate the stagnation point position along the outlet channels with high precision. Here, the on-chip valve is not used to gate fluid flow in a binary (on/off) fashion; rather, it functions as a metering valve for fine-scale adjustment of the relative flow rates in the outlet channels. Closing this valve, for instance, would increase the flow resistance and reduce the flow rate through the outlet channel, which consequently re-positions the stagnation point position towards the same outlet channel.

In this work, we implement a linear feedback controller for particle trapping. Using this control algorithm, the stagnation point is re-positioned to a distance linearly proportional to the displacement offset between the particle and trap center (ESI†). The hydrodynamic force exerted on a point particle is linearly proportional to fluid velocity and therefore linearly proportional to the distance between the particle and the stagnation point along the extensional axis (eqn (1)), which is a consequence of viscous-dominated laminar flow in the microchannels. The linearity in hydrodynamic force with particle displacement aids in implementing a simple linear feedback control algorithm for particle trapping.

Experimental

Device design and fabrication

We built the hydrodynamic trap by designing and fabricating a hybrid poly(dimethylsiloxane) (PDMS)/glass microfluidic device using standard multilayer soft-lithography techniques (Fig. 1a and b).[34] The hydrodynamic trap is a two-layer microfluidic device consisting of two patterned layers in PDMS. A thin PDMS layer (fluidic layer) containing the flow channels (inlet, outlet and sample microchannels) is sandwiched between a glass substrate and a thick PDMS layer (control layer). The control layer contains an elastomeric membrane valve, which consists of a pressurized microchannel positioned above one of the outlet channels. The fluidic layer consists of four buffer inlet channels, two outlet channels and a sample inlet channel. Two buffer inlet streams on each half of the device converge to form two opposing inlet streams, which meet at the cross-slot microchannel junction. The sample inlet stream is introduced through a separate port and is focused between two adjacent inlet buffer streams, thereby delivering particles to the center of the microchannel junction (trapping region). Typical channel dimensions range between 100 and 500 μm in width and 10 and 50 μm in height.

The elastomeric membrane valve is an essential component of the microfluidic-based hydrodynamic trap. The valve consists of a microchannel positioned above one of the outflow channels downstream of the cross-slot configuration and is separated from the flow channels by a thin (20–100 μm) elastomeric (PDMS) membrane. By applying pressure to the control layer microchannel (valve), the membrane is deflected downwards onto the flow channel, thereby changing the cross-sectional area and altering the flow resistance within the outlet stream situated beneath the valve. In this manner, the monolithic membrane valve serves as an on-chip metering valve capable of adjusting the relative flow rates in the outlet channels, which enables fine-scale control of the stagnation point position and facilitates particle confinement. In addition, a constriction is fabricated in the opposite outlet channel, which requires a constant offset pressure to be applied to the membrane valve in order to maintain the stagnation point in the center of the cross-slot. In this work, we demonstrate device operation using a single membrane valve in one of the outlet channels, thereby enabling particle confinement.

The fluidic and control layers are individually patterned in PDMS as two separate layers by replica molding. The molds for the two layers were prepared by spin coating a thin layer (10–50 μm) of negative photoresist (SU-8) onto silicon wafers (3″ diameter) and patterning with UV exposure using a high-resolution transparency film as a mask. The molds are developed with propylene glycol methyl ether acetate (PGMEA) followed by surface treatment with trichlorosilane vapor under vacuum to prevent the adhesion of cured PDMS. Next, the thin fluidic layer is obtained by spin coating the fluidic mold with PDMS at 20 : 1 (w/w) base : crosslinker ratio yielding a thickness of ~70 to 110 μm. Depending on the channel height (10–50 μm), spin coating results in a ~20 to 100 μm thick membrane between the control and fluidic layers. The control layer is formed by casting a thick layer (4–6 mm) of PDMS with 5 : 1 (w/w) base : crosslinker ratio on the corresponding control layer mold. Next, each PDMS layer was partially cured by baking at 70 °C for 30 minutes. The thick PDMS replica (control layer) is then peeled from the control mold, aligned and hermetically sealed onto the thin PDMS layer (fluidic layer) by baking together overnight at 70 °C to form a monolithic device. The PDMS replica containing the two device layers is peeled off the fluidic mold and access ports for the microchannels in both layers are punched out using

a blunt needle. Finally, the PDMS slab is bonded to a coverslip by plasma oxidation to yield a functional device.

Experimental setup and trapping algorithm

The experimental setup consists of the microfluidic device (hydrodynamic trap) mounted on the stage of an inverted microscope (Olympus IX71) equipped with a CCD camera for image acquisition and a 10× or 40× high numerical aperture objective lens for particle detection. A syringe pump (Harvard Apparatus) is used to deliver fluid into the device, and an electronic pressure regulator (Proportion Air) is used to actuate the membrane valve. Particles are trapped using an automated feedback control mechanism. A custom LabVIEW code executes the following steps in the feedback control algorithm: (1) capturing an image of the particles in the trapping region, (2) tracking and localizing the center-of-mass position of a "target" particle in the trapping region, (3) calculating the displacement offset between the particle and trap center and determination of the pressure required for the on-chip valve using a linear feedback controller, (4) signalling the pressure transducer to apply an updated pressure to the on-chip valve, which adjusts the stagnation point position to steer the trapped particle towards the trap center. In this work, the duration of one cycle of the feedback loop is 60–140 ms (7–15 Hz feedback loop rate), which efficiently confines particles at the trap center.

Results and discussion

Particle trapping

Using the microfludic trap, we confined micro- and nanoscale particles (100 nm–15 μm diameter) for long timescales (minutes) in free-solution. In addition, we trapped both fluorescent and non-fluorescent beads and single cells (bacterial and mammalian) using the device. Fig. 2a shows the trajectory of a trapped particle (2.2 μm diameter fluorescent polystyrene bead) confined for nearly 5 minutes in the microchannel junction. Fig. 2b and c show the histogram of bead displacement from the trap center along the inlet and outlet channel directions, respectively. The trajectory of a trapped particle may be obtained by either using the centroid position data recorded by the LabVIEW code, or by tracking and localizing the trapped particle from the recorded movie of the trapping region.

Particles are trapped "on-demand" such that the user can continue to trap a "target" particle or simply release the trapped object by terminating the feedback controller and select a new target particle. Selection of a new "target" particle is accomplished using a manual or automated scheme based on particle properties (*e.g.*, size and morphology). For example, particles matching a desired size and morphology criteria can be identified *via* custom pattern recognition and particle measurement algorithms in LabVIEW and subsequently confined at the trapping region for further observation and analysis. In addition, a trapped particle can be manipulated by translating the trap center position. In this case, the stagnation point position is adjusted to steer the particle and ultimately confine it at the new desired trap center. Using the feedback control algorithm, microscale particles are confined to within ±1 μm of the trap center along the inlet and outlet channel directions.

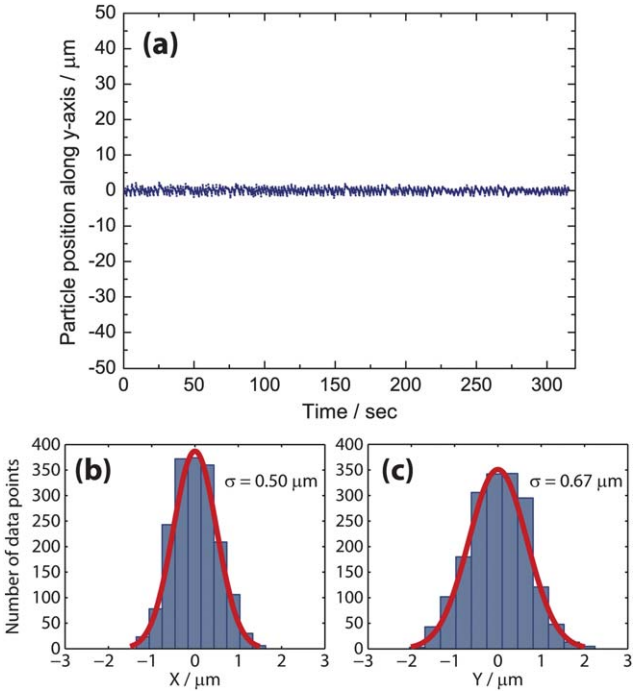

Fig. 2 Particle trapping. (a) Trajectory of a trapped particle (fluorescent bead, 2.2 μm diameter) in a direction parallel to the outlet stream direction. The bead is confined to within ±2 μm for nearly 5 minutes. (b and c) Histogram of displacements for the trapped bead (2.2 μm diameter) from the trap center along the inlet and outlet streams respectively. σ is the standard deviation of displacements from the trap center.

Stagnation point position

Particle confinement and manipulation is achieved through precise control of the stagnation point position, which, in turn, is adjusted using an integrated on-chip valve. Therefore, the effect of valve pressurization on the stagnation point position will determine the overall trap performance.

In order to design and engineer a robust microfluidic-based trap, we systematically analyzed the response mechanism for each step in the trapping process. The overall process flow scheme for hydrodynamic trapping is summarized by the following steps (Fig. 3).

(1) On-chip membrane valve is pressurized.
(2) Cross-sectional area of the valve changes.
(3) Relative flow resistance in outlet channels change.
(4) Stagnation point position moves to a new location.
(5) Particle moves toward trap center *via* an updated force.

In this article, we model each step in the trapping process with regard to microfluidic device design parameters in order to quantify trap response. For each step, we develop a theoretical model and provide experimental validation of overall device performance. We analyze device parameters directly impacting control of stagnation point position, including the membrane valve design parameters, such as the width, height and the length of the constriction. In addition, we examine the structural characteristics of the membrane valve, such as the membrane thickness and stiffness *via* the PDMS base-to-crosslinker ratio.

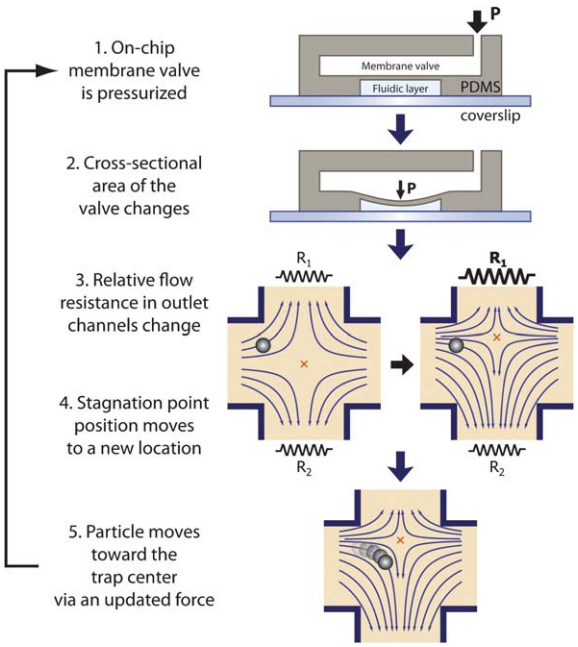

Fig. 3 Hydrodynamic trap mechanism. Schematic of hydrodynamic trap mechanism showing overall process flow for particle confinement by control of stagnation point position using an integrated on-chip valve.

The effect of membrane valve pressurization on valve cross-sectional area

Membrane deflection changes the cross-sectional area of the fluidic channel beneath the control layer, thereby adjusting the relative flow resistance in one outlet channel with respect to the other (Fig. 4a). In this manner, the control layer acts as a dynamic metering valve controlling flow rates in the fluidic layer, which enables the fine-scale control of stagnation point position. The response of the valve against applied pressure depends on the physical properties of the membrane, such as membrane thickness and stiffness. In order to fully characterize valve response, we fabricated microfluidic devices with varying membrane thickness (d = 31, 37, 51 and 66 μm) between the control and the fluidic layer. We characterized the effect of membrane thickness on valve function by measuring the valve opening for several pressure values (0–130 kPa) applied to the membrane. Previous work reported valve response in the context of binary on/off valves.[35] Here, we characterize valve response in the context of dynamic metering valves for hydrodynamic trapping, which is essential for optimal device performance. To determine valve opening at a specific pressure value, the microchannel in the fluidic layer is filled with a fluorescent dye solution, and the section of the microchannel under the membrane valve is imaged by a CCD camera at variable pressure. Valve opening is determined by calculating the ratio of the total fluorescence intensity under the membrane valve at a given pressure relative to zero applied pressure (fully open).

Valves with thinner membranes close at relatively low pressure values compared to those with thicker membranes (Fig. 4b). Valves with thicker membranes are less responsive, though they exhibit a wider range of linear response against changes in pressure. For instance, the membrane valve shows a linear

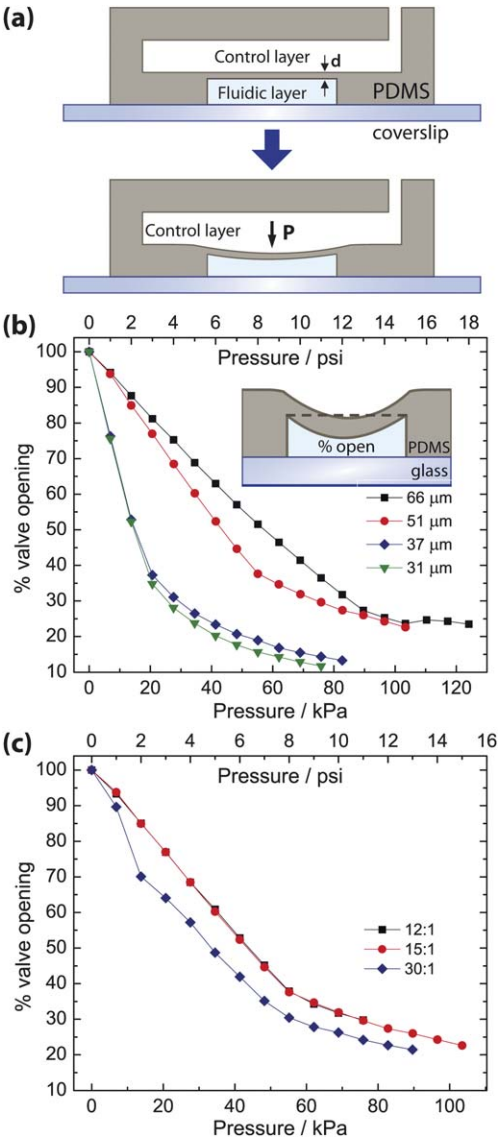

Fig. 4 Membrane valve characterization. (a) Schematic of membrane valve operation. The control layer contains a pneumatic membrane valve which is used to adjust the flow rates in the fluidic layer, thereby enabling manipulation of the stagnation point position. A thin elastomeric membrane (d = 30–70 μm) separates the control layer and the fluidic layer and is deflected downwards onto the fluidic layer by applying pressure to the control layer, which changes the relative flow rates in the outlet channels. (b) Valve response for four different membrane thicknesses. As the membrane thickness is reduced, the valve becomes more responsive to pressure changes. (c) Valve response for three different PDMS base-to-crosslinker ratios (12 : 1, 15 : 1 and 30 : 1) for the fluidic layer. As the crosslinker amount is reduced, the valve becomes more responsive. Error bar sizes are on the order of the size of the data points.

response range between 0 and 20 kPa, and 0 and 90 kPa for 31 and 66 μm membrane thicknesses, respectively. A wide range of linear valve response represents an important design advantage for valve control, as it facilitates implementation of a linear (proportional) feedback control algorithm for particle trapping. In this work, we used "push-down" valves on microchannels with rectangular cross-sections such that the membrane valves are not able to fully close the microchannels. In the context of

a hydrodynamic trap, inability to fully close valves is not a disadvantage *per se* because membrane valves are utilized as metering valves (typically within the linear response range) rather than binary on/off valves.

We also characterized the effect of membrane stiffness on valve performance. Here, we varied PDMS base : crosslinker ratio and studied valve function by measuring valve opening for several pressure values (0–110 kPa) applied to the membrane (Fig. 4c). A two-layer PDMS device is fabricated by bonding two PDMS device layers containing excess amounts of either base or crosslinker. We used a 5 : 1 base : crosslinker ratio for the control layer and 12 : 1, 15 : 1 and 30 : 1 ratios for the fluidic layer, which contains the membrane portion of the on-chip valve. During the curing process, the base : crosslinker ratio shifts towards a ~10 : 1 ratio at the interface of the two layers due to the diffusion of excess crosslinker across the layers. However, the desired target ratios of 12 : 1, 15 : 1 and 30 : 1 are retained within the membrane valve, because microchannels are situated immediately above and below the membrane, and the membrane does not come into conformal contact with the control layer. Therefore, the membrane valve is expected to become increasingly flexible and more responsive with increasing base : crosslinker ratio in the fluidic layer. Indeed, as the base : crosslinker ratio in the fluidic layer is increased from 12 : 1 to 30 : 1 (Fig. 4c), the membrane valve becomes more responsive, *i.e.* the change in valve opening per unit pressure change increases.

Effect of valve cross-sectional area on the relative flow rates through the outlet channels

In the hydrodynamic trap, the on-chip membrane valve is used to adjust flow resistance by forming a variable constriction within one of the outlet channels, resulting in an overall change in the relative flow rates distributed through both outlet channels.

The flow resistance within an outlet channel can be adjusted using a constriction that changes the cross-sectional area along the height or width of the channel (or both). For a microchannel with rectangular cross-section, the flow resistance is an asymmetric function of channel height and width with a stronger dependence on the former (see ESI†). Therefore, a unit change in channel height and width along the constriction would yield different overall flow resistances for the outlet channel (see Fig. 5 and discussion below). Depending on the desired response, membrane valves can be designed to induce a constriction along either the height or width of the cross-sectional area of the channel.[34,36] In order to study the effect of changing the constriction width on flow resistance, we designed and built a series of model devices with varying constriction widths. In addition, in order to characterize the effect of changing the constriction height on flow resistance, we employed push-down membrane valves to induce changes in the channel height.

Before embarking on experiments, we theoretically modelled the membrane valve as a constriction with either variable height (h_v) or variable width (w_v) located in one of the outlet channels (Fig. 5a and b, see ESI†). We derived the fluid equations describing the dependence of Q_v/Q_{tot} on the variable constriction width (w_v), height (h_v) and length (L_v) by calculating the flow resistances of each outlet channel, and the results are plotted in Fig. 5c. Overall, the relative flow rate (Q_v/Q_{tot}) exhibits

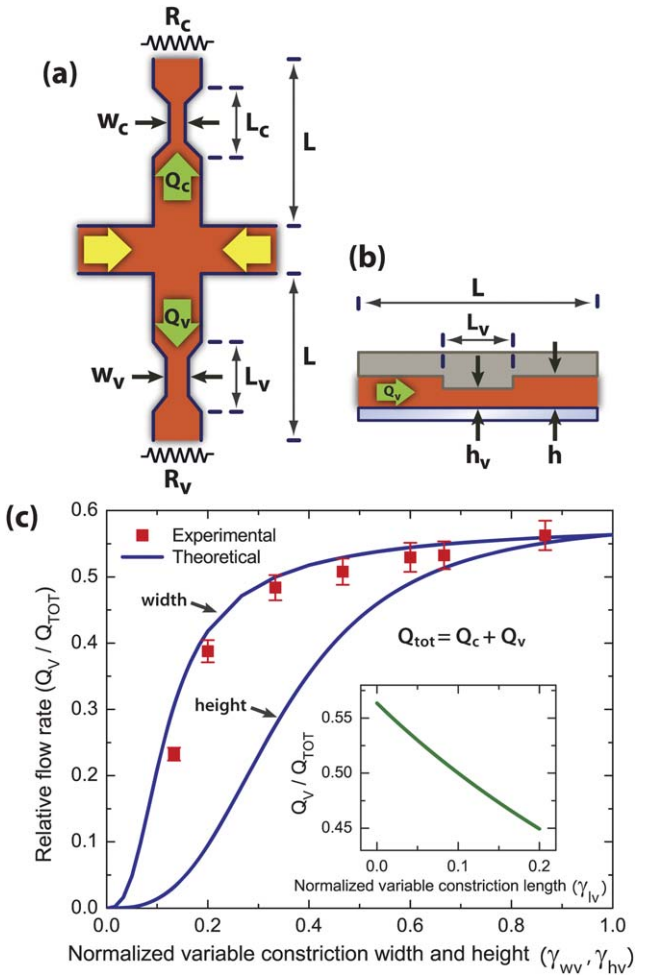

Fig. 5 Device design: the effect of valve cross-sectional area on the relative flow rates. (a) Device layout showing one fixed and one variable constriction situated on opposing outlet channels. Here, the channel width is modelled as the variable parameter for the constriction. (b) The channel height can also be modelled as the variable parameter for the constriction. (c) For device configurations illustrated in a and b, the theoretical ratio of flow rates through the outlet channel with the variable constriction (Q_v) to the total flow rate (Q_{tot}) as a function of normalized variable constriction width (γ_{wv}), height (γ_{hv}) and length (γ_{lv}) is shown. Flow rates (Q_v/Q_{tot}) were also experimentally measured for seven devices with different variable constriction width. For these devices, one of the outlet channels had a fixed constriction width ($w_c = 100$ μm) whereas the other outlet channel had a variable constriction width ($w_v = 40$–260 μm). Constriction widths (w_c,w_v = 0–300 μm), height (h_v = 0–50 μm) and lengths (L_c = 1 mm, L_v = 0–2 mm) are normalized to the outlet channel width (w = 300 μm), height (h = 50 μm) and length (L = 10 mm) respectively. Experimental data at seven different variable constriction width values show good agreement with the theoretical curve. The flow splits equally at $\gamma_{wv} = \gamma_{we} = 0.333$, *i.e.* $w_v = w_c = 100$ μm, such that $Q_c = Q_v$ and $Q_v/Q_{tot} = 0.5$. (Inset) The outlet channel flow resistances increase nearly linearly with the constriction length (L_c or L_v) leading to a linear decrease in the flow rate ratio.

a sigmoidal response as a function of normalized variable constriction width and height. Locally, and for small changes in the constriction dimension, the flow rate partitioning function Q_v/Q_{tot} can be modelled as a linear function of normalized variable constriction width or height, which facilitates

implementing a linear proportional feedback controller for particle trapping. Q_v/Q_{tot} decreases nearly linearly as a function of normalized variable constriction length. In addition, results from these calculations suggest that relatively small changes in the volumetric flow rate partitioning occur for partially open or nearly fully open valves, whereas large changes occur for nearly closed valve positions (Fig. 5c).

To experimentally characterize the response of actual membrane valves, we first designed and built a series of model devices with varying constriction widths. These devices contain constrictions with varying width (w_v) located on one of the outlet channels, as shown in Fig. 5a. The opposing outlet channel contains a constriction with a fixed width (Fig. 5a, $w_c = 100$ μm), which is also included in the actual hydrodynamic trap device. We fabricated microfluidic devices with seven different variable constriction widths ($w_v = 40$, 60, 100, 140, 180, 200 and 260 μm) and measured the ratio of the flow rate through the outlet channel containing the variable constriction (Q_v) to the total flow rate (Q_{tot}) as a function of the variable constriction width (w_v) (Fig. 5c). Flow rates are experimentally determined by particle tracking measurements (see ESI†). For model devices, the flow rate partitioning function Q_v/Q_{tot} shows good agreement between experimental data and theory when Q_v/Q_{tot} is plotted as a function of the variable constriction width normalized to the microchannel width ($\gamma_{wv} = w_v/w$). Finally, we experimentally determined the effect of changing constriction height on fluid flow by directly measuring stagnation point position, as discussed in subsequent sections (Fig. 6).

Is the action of membrane valves in actual devices better described by channel constrictions varying in width or height? For actual hydrodynamic trap devices with push-down membrane valves, our results suggest membrane valves are more accurately modelled by changes in constriction channel height, as discussed in the following section (see Fig. 6). In general, push-down membrane valves induce non-uniform changes in both channel height and width. However, valve opening exhibits a linear response over a wide range of applied pressures used in particle trapping (Fig. 4b and c), thereby suggesting that channel height changes linearly during actual device operation.

Effect of relative flow rates in the outlet channels on stagnation point position

Inlet fluid streams approach the cross-slot junction along the compressional flow direction and split into two opposing outlet streams (Fig. 6a and b, and S3, ESI†). For equally balanced volumetric flow rates within the inlet and outlet channels, the stagnation point is located at the center of the cross-slot junction. Varying the relative flow rates within the two outlet channels effectively moves the stagnation point along a line parallel to the outflow direction. At any instant in time, the stagnation point is located on the partition line at which the inlet streams split and flow into the two outlet channels (Fig. 6b). Therefore, the position of the stagnation point intrinsically determines the flow rates exiting through each outlet channel. In order to model the location of the stagnation point as a function of membrane valve position, we calculated the ratio of the flow rate exiting one outlet channel relative to the total flow rate (Q_v/Q_{tot}) as a function of the stagnation point position (see ESI†). The results suggest that the incoming flow splits nearly linearly with the stagnation point position (Fig. S3, ESI†). The flat (plug-like) fluid velocity profile in the inlet and outlet channels (Fig. S1c†), as well as the fluid

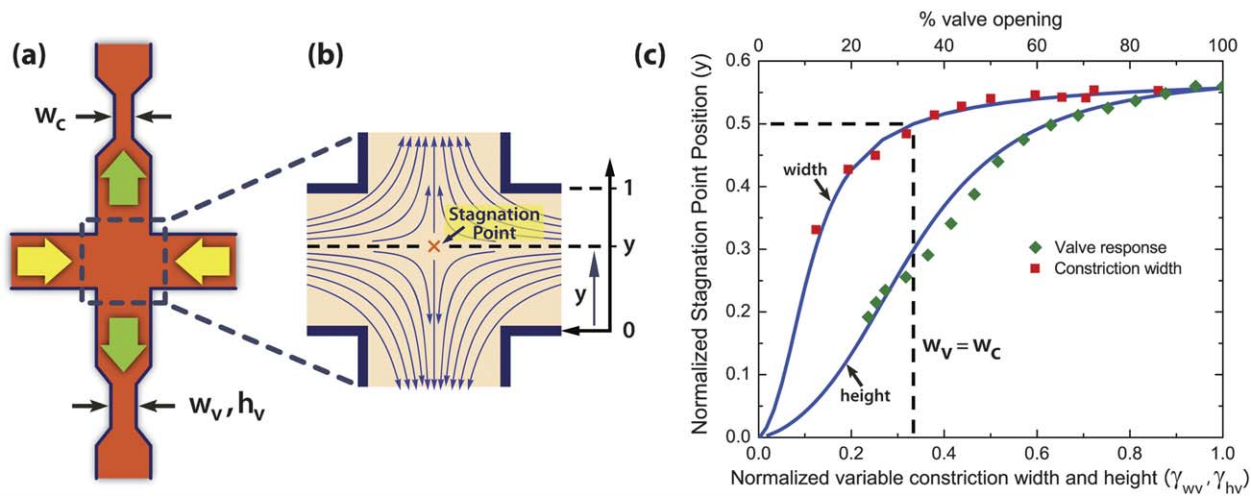

Fig. 6 Device design: channel constriction width and height. Fluid stagnation point position as a function of constriction width and height was determined. (a) One constriction in each outlet channel is used to manipulate the position of the stagnation point position. One of the outlet channels has a fixed constriction ($w_c = 100$ μm) whereas the other outlet channel has a variable constriction width ($w_v = 40$–260 μm). (b) As the variable constriction size (width or height) is changed, the position of the stagnation point is effectively moved along the outlet channels. (c) Theoretical (solid line) and experimental (squares, diamonds) data for the stagnation point position change with constriction size. We built microfluidic devices with 12 different variable constriction widths and measured the normalized stagnation point position (squares). The variable constriction width (w_v) and the stagnation point position are normalized to the microchannel width ($w = 300$ μm). At ($\gamma_{wv} = \gamma_{wc} = 0.333$, *i.e.* $w_v = w_c = 100$ μm), the flow is split equally and the stagnation point is located at the center of the channel. The effect of membrane valve opening on the stagnation point position shows a response curve similar to the theoretical response curve for changes in constriction height, thereby suggesting that the membrane valve mainly induces a change in channel height along the outlet channel.

velocity profile in the vicinity of the stagnation point (eqn (1)), result in the linear relationship between flow rate partitioning and stagnation point position. Near the channel walls (within 10% of the channel width), the fluid velocity approaches zero, resulting in deviations from the linear response (Fig. S3†).

Overall, precise regulation of the relative flow rates through the outlet channels enables linear, fine-scale adjustment of the stagnation point position at the microchannel junction. Furthermore, the linear relationship allows for control of stagnation point position using a linear feedback controller. In this way, a flow rate increase in one of the outlet channels would move the stagnation point away from this channel outlet in a linear fashion.

Effect of valve cross-sectional area on stagnation point position

As a final step in modelling the microfluidic-based trapping mechanism, we characterize the effect of valve cross-sectional area on stagnation point position using a model system and actual trap devices. Overall, these experiments build on the knowledge of valve response presented in Fig. 5 by quantifying the stagnation point response as a function of valve constriction width and height.

First, we calculated the theoretical dependence of the stagnation point position as a function of the variable constriction width (w_v) and height (h_v) by combining the dependence of the relative flow rates through outlet channels (Fig. 5) with the effect of the relative flow rates on stagnation point position (Fig. S3†). As the variable constriction width changes, the position of the stagnation point effectively moves along the principal axis of extension (axis parallel to the outlet channels as shown in Fig. 6b and c). Results describing the response of the stagnation point position to changes in the variable constriction width are presented in Fig. 6c. Overall, the fluid stagnation point position exhibits a sigmoidal response to changes in the variable constriction width. As expected, the stagnation point is located at the center of the channel when the constriction widths for both outlet channels are equal (*i.e.* $w_v = w_c$), thereby resulting in equal flow partitioning.

To experimentally characterize changes in the stagnation point position as a function of constriction width, we fabricated devices with 12 different variable constriction widths (w_v = 40–260 μm as shown in Fig. 6a) and experimentally measured the fluid stagnation point position. In these model devices, one of the outlet channels has a fixed constriction (w_c = 100 μm), whereas the width of the variable constriction (w_v) on the opposite outlet channel is changed. Experimental results are shown in Fig. 6c and agree well with theoretical calculations. Experimental determination of the stagnation point position is accomplished by particle tracking as described in the ESI† (Fig. S4).

Finally, we examined the actual response of the stagnation point position against membrane valve opening in functional hydrodynamic trap devices. Here, we varied the pressure applied to the membrane valve and measured the stagnation point position by particle tracking. As shown in Fig. 6c, the stagnation point response to changes in valve opening is sigmoidal for functional trap devices. The experimental response curve suggests that the membrane valve acts as a constriction decreasing in height with increasing applied pressure. For this analysis, the applied pressure is converted to a percent valve opening using experimental data shown in Fig. 4b and c. Results shown in Fig. 6 suggest that the constriction formed by the membrane valve is accurately modelled by variations in constriction channel height rather than channel width, which might be explained by the relatively low aspect ratios in our microchannels ($0.1 < \alpha < 0.166$). In addition, the channel width (w = 300 μm) is significantly smaller than the constriction length (L_c = 1 mm), thereby resulting in more uniform changes in the channel height with valve closure along the channel length.

Conclusion

The hydrodynamic trap facilitates particle confinement and manipulation using a stagnation point flow generated in a cross-slot microfluidic device. Particles are confined at a user-defined set point (trap center) using an automated feedback control mechanism. The feedback controller continuously tracks particle position and adjusts stagnation point position using an integrated on-chip metering valve. Using the hydrodynamic trap, particles are confined in free-solution at a stagnation point, whereas the vast majority of existing microfluidic methods for particle manipulation relies on physical barriers (which necessitate particle-wall contact), circulating flows or microeddies. Overall, the microfluidic-based hydrodynamic trap offers a new method for non-contact and free-solution confinement of arbitrary particles or cells for long time scales.

In this work, we investigate the hydrodynamic trap response as a function of microfluidic device design parameters, including membrane valve characteristics and channel dimensions. We developed a model for stagnation point response as a function of applied valve pressure and validated the theoretical model with experiments. Overall, the model describing the on-chip membrane valve enables quantitative understanding of valve response. Furthermore, precise understanding of stagnation point position as a function of valve response will allow for design and implementation of robust hydrodynamic traps for tailored applications, including confinement of small nanoparticles and manipulation of arbitrary particles in flow. Selecting and implementing specific valve design parameters will enable custom engineering of the on-chip membrane valve and facilitate rational design of the trap response. For example, one can envision designing a hydrodynamic trap with a response curve with a given slope and linear response region for trapping applications specific to "target" particles or cells.

In this manuscript, we characterize key design parameters determining the response of the stagnation point to changes in the applied valve pressure. By combining experiments and theory, we develop a quantitative model for the microfluidic-based hydrodynamic trap and provide a general framework for building and implementing an effective model-based control algorithm. The experiments described in this paper utilize a linear feedback control algorithm for particle trapping. However, custom model-based feedback controllers utilizing valve response curves for any microdevice trap design may be implemented in the hydrodynamic trap.[37]

Although we used a push-down (or actuate-to-close) valve that mainly changes the microchannel height in this work, a valve that changes the microchannel width can also be employed.[36] In this

way, a hydrodynamic trap with a tailored response can be achieved. Implementation of valves with well-characterized response curves would allow for custom trap design for specific particle trapping applications.

The microfluidic trap offers several advantages for the confinement and manipulation of micro and nanoscale particles. First, particles are trapped in free-solution, thereby allowing for non-perturbative and non-contact confinement of single particles or cells. In addition, trapping is achieved by the sole action of hydrodynamic flow, thereby eliminating the need for optical, electric, magnetic or acoustic fields. Hydrodynamic trapping is possible for any arbitrary particle with no specific requirements on material composition or chemical/physical properties (*e.g.* surface charge, refractive index) of the trapped object. Furthermore, single particles may be hydrodynamically trapped in a concentrated solution of particles, which enables confinement, micromanipulation and isolation of a single target particle in a crowded solution, difficult to achieve using alternative force field trapping methods. In addition, hydrodynamic trapping allows for dynamic exchange of the surrounding medium (pH, temperature, ion concentration, *etc.*) of a trapped particle, coupled with concomitant and direct imaging for real-time characterization of single nanoparticles or cells. Finally, hydrodynamically trapped particles may be monitored using a wide variety of microscopy techniques including bright field, phase contrast and fluorescence microscopy. Overall, the microfluidic-based hydrodynamic trap offers a powerful and versatile platform for non-perturbative, fine-scale confinement and manipulation of micro and nanometre-sized particles for long-time observation without surface immobilization.

Acknowledgements

We thank Prof. Paul J. A. Kenis and his group for providing access to cleanroom facilities for microdevice fabrication. This work was funded by an NIH Pathway to Independence (PI) Award, under Grant No. 4R00HG004183-03.

References

1 A. Ashkin, J. M. Dziedzic, J. E. Bjorkholm and S. Chu, *Opt. Lett.*, 1986, **11**, 288–290.
2 K. C. Neuman and S. M. Block, *Rev. Sci. Instrum.*, 2004, **75**, 2787–2809.
3 D. G. Grier, *Nature*, 2003, **424**, 810–816.
4 A. H. J. Yang, S. D. Moore, B. S. Schmidt, M. Klug, M. Lipson and D. Erickson, *Nature*, 2009, **457**, 71–75.
5 P. Y. Chiou, A. T. Ohta and M. C. Wu, *Nature*, 2005, **436**, 370–372.
6 A. E. Cohen and W. E. Moerner, *Appl. Phys. Lett.*, 2005, **86**, 093109.
7 A. E. Cohen, *Phys. Rev. Lett.*, 2005, **94**, 118102.
8 A. Ramos, H. Morgan, N. G. Green and A. Castellanos, *J. Phys. D: Appl. Phys.*, 1998, **31**, 2338–2353.
9 C. Gosse and V. Croquette, *Biophys. J.*, 2002, **82**, 3314–3329.
10 H. Lee, A. M. Purdon and R. M. Westervelt, *Appl. Phys. Lett.*, 2004, **85**, 1063–1065.
11 H. M. Hertz, *J. Appl. Phys.*, 1995, **78**, 4845–4849.
12 M. Evander, L. Johansson, T. Lilliehorn, J. Piskur, M. Lindvall, S. Johansson, M. Almqvist, T. Laurell and J. Nilsson, *Anal. Chem.*, 2007, **79**, 2984–2991.
13 G. I. Taylor, *Proc. R. Soc. London*, 1934, **146**, 501–523.
14 B. J. Bentley and L. G. Leal, *J. Fluid Mech.*, 1986, **167**, 219–240.
15 T. T. Perkins, D. E. Smith and S. Chu, *Science*, 1997, **276**, 2016–2021.
16 C. M. Schroeder, H. P. Babcock, E. S. G. Shaqfeh and S. Chu, *Science*, 2003, **301**, 1515–1519.
17 S. D. Hudson, F. R. Phelan, M. D. Handler, J. T. Cabral, K. B. Migler and E. J. Amis, *Appl. Phys. Lett.*, 2004, **85**, 335–337.
18 P. R. Start, S. D. Hudson, E. K. Hobble and K. B. Migler, *J. Colloid Interface Sci.*, 2006, **297**, 631–636.
19 J. S. Lee, R. Dylla-Spears, N. P. Teclemariam and S. J. Muller, *Appl. Phys. Lett.*, 2007, **90**, 074103.
20 M. D. Armani, S. V. Chaudhary, R. Probst and B. Shapiro, *J. Microelectromech. Syst.*, 2006, **15**, 945–956.
21 B. R. Lutz, J. Chen and D. T. Schwartz, *Anal. Chem.*, 2006, **78**, 5429–5435.
22 C. M. Lin, Y. S. Lai, H. P. Liu, C. Y. Chen and A. M. Wo, *Anal. Chem.*, 2008, **80**, 8937–8945.
23 R. Dylla-Spears, J. E. Townsend, L. Jen-Jacobson, L. L. Sohn and S. J. Muller, *Lab Chip*, 2010, **10**, 1543–1549.
24 M. Tanyeri, E. M. Johnson-Chavarria and C. M. Schroeder, *Appl. Phys. Lett.*, 2010, **96**, 224101.
25 R. M. Johann, *Anal. Bioanal. Chem.*, 2006, **385**, 408–412.
26 J. Nilsson, M. Evander, B. Hammarstrom and T. Laurell, *Anal. Chim. Acta*, 2009, **649**, 141–157.
27 D. Di Carlo and L. P. Lee, *Anal. Chem.*, 2006, **78**, 7918–7925.
28 D. Di Carlo, L. Y. Wu and L. P. Lee, *Lab Chip*, 2006, **6**, 1445–1449.
29 J. R. Rettig and A. Folch, *Anal. Chem.*, 2005, **77**, 5628–5634.
30 J. Seo, C. Ionescu-Zanetti, J. Diamond, R. Lal and L. P. Lee, *Appl. Phys. Lett.*, 2004, **84**, 1973–1975.
31 J. Sinclair and A. K. Salem, *Biomaterials*, 2006, **27**, 2090–2094.
32 W. H. Tan and S. Takeuchi, *Proc. Natl. Acad. Sci. U. S. A.*, 2007, **104**, 1146–1151.
33 A. M. Skelley, O. Kirak, H. Suh, R. Jaenisch and J. Voldman, *Nat. Methods*, 2009, **6**, 147–152.
34 M. A. Unger, H. P. Chou, T. Thorsen, A. Scherer and S. R. Quake, *Science*, 2000, **288**, 113–116.
35 V. Studer, G. Hang, A. Pandolfi, M. Ortiz, W. F. Anderson and S. R. Quake, *J. Appl. Phys.*, 2004, **95**, 393–398.
36 A. R. Abate and D. A. Weitz, *Appl. Phys. Lett.*, 2008, **92**, 243509.
37 D. E. Seborg, T. F. Edgar and D. A. Mellichamp, *Process Dynamics and Control*, Wiley, Hoboken, NJ, 2004.

